NUCLEAR GROUND STATE PROPERTIES AND SELF-CONSISTENT CALCULATIONS WITH THE SKYRME INTERACTION

II. S-D SHELL NUCLEI

H. FLOCARD

Institut de Physique Nucléaire-Division de Physique Théorique
91406-Orsay-France

and

P. QUENTIN

Institut de Physique Nucléaire-Division de Physique Théorique
91406-Orsay-France
and
Niels Bohr Institute-2100 Copenhagen Ø-Denmark

IPNO-PHY 75-11

NUCLEAR GROUND STATE PROPERTIES AND SELF-CONSISTENT CALCULATIONS WITH THE SKYRME INTERACTION

II. S-D SHELL NUCLEI

H. FLOCARD
Institut de Physique Nucléaire-Division de Physique Théorique[+]
91406-Orsay-France

and

P. QUENTIN
Institut de Physique Nucléaire-Division de Physique Théorique[+]
91406-Orsay-France
and
The Niels Bohr Institute-2100 Copenhagen Ø-Denmark

IPNO/TH 75-11 April 1975

[+]Laboratoire associé au C.N.R.S.

Abstract

We present and discuss Hartree-Fock results concerning the ground state properties of some S-D shell nuclei. Two different Skyrme interactions have been used. They both lead to good agreement with the experimental total binding energies, charge radii and multipole moments. In particular the observed prolate-oblate transitions occuring in the S-D shell are reproduced. The calculated spectroscopic factors are also shown to be consistent with experimental data.

1. Introduction

The wealth of experimental data has stimulated a great number of theoretical studies on the nuclei of the S-D shell. Another reason for this interest is the small number of nucleons in these nuclei which makes calculations easier. One class of investigations consists of very elaborate shell model calculations (see e.g. Refs.[1]). A second important group is concerned with various kinds of self-consistent methods. Among them the simplest ones correspond to pure Hartree-Fock (H.F.) (Refs.[2-5]) or Hartree-Fock Bogolyubov calculations [6] . During the last years a great effort has been devoted to investigate the effects of the projection (after or before variation) on states of either definite angular momentum or number of nucleons [6-8] . Finally one can also mention recent calculations [9] performed according to the Strutinsky prescription although for such light nuclei they are not a priori free of fundamental ambiguities.

In this paper we report the results of simple deformed H.F. calculations using the Skyrme interaction for eight S-D shell nuclei. Although they are less elaborate than many of those which we have quoted it is our opinion that they are of interest nevertheless for several reasons :

i) A recent study of the Skyrme parametrization [10] has shown that there exists a priviligied family of parameter sets for the Skyrme interaction. The H.F. calculations on all magic nuclei performed with any interaction belonging to this family reproduce the experimental total binding energies within one or two MeV. Moreover the electron scattering cross-sections which are deduced from the corresponding H.F. charge distributions agree well with experiment. The interactions in this family differ mainly in the predicted non locality of the self consistent field or equivalently in the density of the single-particle spectrum. However the experimental information in single-particle spectra cannot be used to determine uniquely the optimal set of force parameters : there are indications that the experimental spectra of magic $\pm$ 1 nucleon systems contain a non negligible coupling of individual-particle states with collective modes of the magic nuclei [11] . Therefore it is interesting to see whether calculations of nuclei lying between two shell closures could give an additional criterion to determine the best effective interaction. For this reason we have made H.F. calculations on

S-D shell nuclei with the two Skyrme parameter sets SIII and SIV which give rather different non localities in the H.F. field. The parameters of these two sets are reported in Table 1. We recall that these two forces which have already been used in other nuclear regions have not been readjusted for the present calculations.

ii) In contrast with most of the previous self-consistent calculations, our results have been obtained by an expansion of the H.F. individual wave functions on a basis including a large number (eleven) of deformed oscillator shells ; some calculations include a still larger basis in order to determine with precision the small effect resulting from the truncation. We think that solving the H.F. equations on such a large basis is not superflous in the region of light nuclei. Indeed the differences in mass and radii between experimental and Skyrme H.F. values are of the same order of magnitude as the truncation errors resulting from a solution of the H.F. equations on a basis including only seven oscillator shells.

We will only restrict here to unconstrained H.F. solutions . A constrained HF calculation from the ground state to the asymptotic situation of two separated fragments with equal masses has been already presented for the ^{32}S nucleus [12] .

In the first section we shall present some technical details and consider mainly the effects of truncation. The second section will deal with binding energies and the oblate or prolate character of the shapes of the intrinsic states. In the third section we shall compare some features of the monopole, quadrupole and hexadecapole parts of the density with those deduced from experimental data.

II. Method of calculation

In this article as in Refs. [4] [13-17] we only study deformations for which the nucleus remains axially symmetric and left-right reflection symmetric. The latter restriction which excludes the odd multipole degrees of freedom does not seem to be crucial for the nuclei of the S-D shell at least when one is interested in the properties of the intrinsic ground state. The first restriction is probably more important. Indeed ^{28}Si has often described in terms of a trixial shape (see e.g. Refs. [2,18]). However from our calculation it will turn out that even restricting ourselves

to axially symmetric shapes we can describe with a good accuracy the overall properties of the nuclear ground states in the S-D shell.

In view of the preceeding assumptions it is natural to expand the H.F. individual wave functions in terms of eigenstates of a deformed cylindrical-oscillator. The technical details of the calculation and of the choice of the appropriate oscillator have already been discussed in refs. [4][13] . We only recall here some points concerning the influence of the basis on the results. The cylindrical oscillator basis is determined by two parameters namely the frequencies on the symmetry axis ω_z and on the perpendicular direction $\omega_\perp$. One can equivalently use the following two quantities :

$$b = \left(\frac{m}{\hbar}\right)^{1/2} (\omega_\perp^2 \omega_z)^{1/6} \quad \text{and} \quad q = \frac{\omega_\perp}{\omega_z} \tag{1}$$

where b is the spherical equivalent oscillator parameter and q a deformation parameter. Values of q greater (less) than one correspond to prolate (oblate) shapes of the basis.

The truncation of the expansion basis is determined in the following way : we include all the eigenstates of the cylindrical oscillator with asymptotic quantum numbers $n_\perp$ and n_z verifying the inequality

$$\omega_\perp (n_\perp+1) + \omega_z (n_z+1/2) \leq (\omega_\perp^2 \omega_z)^{1/3} (N+2) \tag{2}$$

The number N thus characterizes the size of the basis. For moderate deformations, prescription (2) is equivalent to the inclusion in the basis of N+1 deformed oscillator shells. In the limit of large values of N, the H.F. results are independent of the parameters q and b. However the convergence rate of the results for increasing N will crucially depend on the specific value chosen for b and q. For this reason it is desirable to work with oscillator shape resembling, as well as possible the shape of the nucleus. Using a basis with N=4 we have determined the optimal parameters which lead to a maximal total binding energy. The results for ten nuclei are reported in Table 2 . The first column of this table shows that b decreases with increasing mass number. This could have been expected since b varies as the inverse of the nuclear radius when the individual H.F. states are constrained to

be pure oscillator states. One can notice a large difference in the value of b between the nuclei ^{24}Mg and ^{26}Mg. This happens, because we have used the same basis to expand the proton and the neutron wave functions. It would be avoided by determining the optimal parameters either with a larger value of N (e.g. N=6) or by using different bases for protons and neutrons.

The total binding energies of the nuclei ^{16}O, ^{20}Ne, ^{36}Ar and ^{40}Ca calculated on a basis including successively 7, 9, 11 and 13 oscillator shells (N=6, 8, 10 and 12) are shown in Table 3 . For the case of ^{20}Ne (^{36}Ar) we have considered the prolate (oblate) H.F. solution. The basis parameters used are those listed in Table 2 . For the nuclei ^{16}O and ^{40}Ca a comparison with exact H.F. results has been made. These exact results are obtained by directly solving the radial H.F. differential equation in configuration space [19] . They are reported in the column labelled $N=\infty$.

As is seen in table 3 the truncation error for a calculation on a seven oscillator shell basis (N=6) lies between 1.35 and 2.34 MeV whereas it does not exceed 400 keV when the basis includes 11 oscillator shells (N=10). As discussed in Ref.[10] our present knowledge of the nuclear effective interaction permits a determination of total binding energies with an accuracy of a few MeV. Therefore it is desirable to use a basis which makes the uncertainties due to truncation as small as possible. For this reason all the calculations whose results are presented below have been performed with a basis containing eleven oscillator shells.

The H.F. wave functions are not translation invariant. One can correct approximately for this fact by substracting from the total binding energy, the energy due to the motion of the center of mass. As was explained in Ref.[5] this can be achieved by substracting the expectation value of the one body part of the center of mass energy and simultaneously performing a slight renormalization of the force parameters. The interactions SIII and SIV have actually been determined in such a way. The coulomb exchange energy is calculated within the Slater approximation. The discussion of Ref.[20] shows that by this method one reproduces in the S-D shell the exact coulomb exchange energy within 5% to 8% and the exact single particle levels within a few hundred keV.

III. Total binding energies

For each nucleus we have calculated the H.F. solution corresponding to both prolate and oblate shapes. As is generally done we have made the following assumption : the intrinsic ground state is the solution with the maximal binding energy. From the results obtained with SIII and SIV, reported in Table 4 , this prescription assigns for both interactions prolate shapes to the nuclei ^{20}Ne, ^{24}Mg and ^{32}S and oblate shapes for ^{28}Si and ^{36}Ar. Actually this sequence of prolate and oblate shapes agrees with that deduced from the measurements of the quadrupole moments of the first 2^+ levels [21 - 23] . Table 4 also contains results for the nuclei ^{22}Ne, ^{26}Mg and ^{34}S. For ^{34}S we have calculated the energy of both oblate and prolate intrinsic states, it is seen that the prolate-oblate transition in the region ^{32}S-^{36}Ar is taking place in ^{34}S. This is consistent with presently available experimental information [24] .

From Table 4 one also notes that the H.F. binding energies ($B_{H.F.}$) are in fairly good agreement with experimental ones (B_{exp}) [25] . The differences $\Delta B = B_{H.F.} - B_{exp}$ are always negative and never exceed 4.5 MeV for SIII and 7.8 MeV for SIV.

Before entering into the discussion of the physical effects which could possibly explain these differences, it is interesting to point out the improvement associated with the use of a deformed basis. Table 5 shows, along with the experimental binding energies of the 4-N nuclei, the differences ΔB as well as the quantities $\Delta B_s = B(\text{spherical H.F.}) - B_{exp}$ for both SIII and SIV. The quantities ΔB_s have been considered in Ref. [10] . It was shown that the interaction SIV gives rise to a strongly non local H.F. field (effective mass in nuclear matter $m^*/m=0.47$). This leads to differences ΔB_s for non magic nuclei larger than those calculated with the force SIII for which the effective mass value is larger ($m^*/m=.76$). This is also seen in Table 5 ; ΔB_s does not exceed 10.5 MeV for SIII whereas it can be as large as 17 MeV for SIV. The difference in the non locality is also reflected in the single particle spectrum which is found more dense with the interaction SIII [10] leading thus to smaller shell effects on the energy. For this reason one should expect the spherical barrier ($\Delta B - \Delta B_s$) to be higher with SIV than with SIII. Indeed for the nucleus ^{24}Mg the value of the spherical barrier is only 7.8 MeV with SIII whereas

it is 12.44 MeV with SIV. The same is true for other nuclei.

For deformed nuclei the H.F. wave function is not an eigenfunction of the total angular momentum J^2 and should rather be considered as the intrinsic state corresponding to the ground-state band. A rough estimate [26] of the difference ΔE between the intrinsic H.F. energy and the energy of the 0^+ ground state is given by

$$\Delta E = \frac{\hbar^2}{2\mathcal{J}} \langle J^2 \rangle \qquad (3)$$

where $\mathcal{J}$ is the moment of inertia and $\langle J^2 \rangle$ the expectation value of the total angular momentum in the H.F. state. Table 6 shows the quantities $\hbar^2/\mathcal{J}$ as extracted from the experimentally known first 2^+ levels [27], the values of $\langle J^2 \rangle$ as well as the differences ΔE. It should be kept in mind however that formula (3) is only valid for pure rotors which is hardly the case here. For this reason and because of the inconsistency of a calculation, which uses both experimental $\mathcal{J}$ and calculated $\langle J^2 \rangle$, the ΔE's of Table 6 must be considered as giving only the order of magnitude of the rotational corrections. It is nevertheless encouraging to see that for both interactions they correspond approximately to the differences ΔB.

IV. Nuclear densities

A) Monopole part of the densities

The root mean square radii of the H.F. charge densities are reported in table 7. They are extracted from the monopole part of the proton density by a convolution with a form factor for the proton. For such light nuclei it is necessary also to take into account the effect of the center of mass motion on the radii [28]. The H.F. radii are systematically larger than the experimental ones [29] but the discrepancy never exceeds 0.07 fm.

A more detailed test of the monopole part of the charge density is provided by elastic electron scattering experiments. In figures 1 and 2 we have reported along with a low energy experimental cross section [30], the differential cross sections deduced by a phase shift analysis from the monopole part of the H.F. charge densities.

In figures 3 and 4 the mean percentage deviation δ of our results for the two nuclei ^{28}Si and ^{32}S has been drawn with :

$$\delta = 200 \times \frac{\sigma_{th} - \sigma_{exp}}{\sigma_{th} + \sigma_{exp}} \qquad (4)$$

In formula (4) σ_{th} and σ_{exp} are respectively the theoretical and experimental differential electron scattering cross sections. The deviation δ is plotted as a function of the "effective" momentum transfer q_{eff} as it is defined in Ref.[30] . For both nuclei the points corresponding to low and medium energy experiment are reported on the same figure. The agreement is reasonably good except for the high momentum transfer region . One can notice that the results given by the two interactions are of a very similar quality. This contrasts with the case of spherical nuclei where SIV does better than SIII [10] , because it gives a better description of the nuclear surface. However for deformed nuclei the surface thickness of the monopole part of the charge density depends on both the surface thickness of the intrinsic charge density and on its deformation. Therefore it is difficult to assign the differences between calculated and experimental cross sections to a specific feature of the charge distribution.

The above results show that our Skyrme H.F. calculations are not able to give perfectly the absolute value of the monopole charge density. The difference $\Delta\rho_c$ however between the charge densities of two neighbouring nuclei is obtained with a better accuracy. This was already the case for the pair of nuclei (^{209}Bi-^{208}Pb) [31] . The quantity $\Delta\rho_c$ for the two nuclei ^{28}Si and ^{32}S calculated in three different ways is reported in Figure 5. The dashed curve has been obtained from a spherical H.F. calculation with the interaction SIII. Its shape has the general appearance of a 2s1/2 orbital density. The two other curves are deduced from deformed H.F. calculations with SIII and SIV. One should not put too much emphasis on the behavior for small radii because of the radial r^2 weighting factor. For radii larger than 1.5 fm the last two curves are very similar. On the other hand they differ significantly from the spherical charge difference. In particular their most external maximum occurs for a smaller radius ($\simeq$3fm instead of 3.7 fm) The reason for this, will be discussed below.

Recently I. Sick has estimated $\Delta\rho_c$ from an analysis of elastic electron scattering data [32] . For radii larger than 1.5 fm, deformed H.F. results obtained with both interactions are in good agreement with his estimates.

We have expanded the single particle wave functions of all the 4-N nuclei on a spherical basis. The results are given in Tables 8 and 9 . Since the radial quantum number cannot be obtained directly from experiment, we have only reported the number of nucleons of a given L and J contained in the intrinsic H.F. ground state. These two tables provide an explanation for the behavior of the differences $\Delta\rho_c$. In the nucleus ^{28}Si one finds more than 2 protons in s1/2 shells showing thus that the 2s orbital is partly filled. Consequently, in the region from ^{28}Si to ^{32}S the number of protons in the 2s1/2 orbital increases by less than 2 units and most of the remaining protons fill the 1d3/2 orbital. This in turn, provides an explanation for the previously noted behavior of the differences $\Delta\rho_c$ because the radius of the 2s1/2 orbital is larger than that of the 1d3/2 *.

Proton spectroscopic factors, extracted [33-34] by a DWBA treatment from d-^{3}He data are shown in table 10 . They are in reasonably good agreement with the results of tables 8 and 9 . It may be worth noticing the presence of 1f7/2 and 1g9/2 components in the ground state of some S-D shell nuclei suggested both by our calculation and by the experimental results . For the sake of completeness the calculated spectra (with SIII) are plotted as a function of A in figures 6 and 7. For deformed nuclei we have plotted the centroid of the levels stemming from a given spherical multiplet. As a consequence of the Coulomb interaction the slope of single proton levels as a function of A is smaller than that of neutron. One can also note that the slope of high and low spin levels inside a shell is different (see e.g. 1d3/2 and 2s1/2 levels).

---

*There is no contradiction between the results of Table 9 (where it is shown that the number of nucleons in s1/2 orbitals increases from ^{28}Si to ^{32}S) and the sign of the difference $\Delta\rho_c(r=0)$ calculated with SIV in Fig. 5. Indeed this sign only shows that the change of the radial wave functions overcompensates the effect of the increase of the proton number.

B) Quadrupole and hexadecapole parts of the densities

In the discussion of the total binding energies we mentioned that our calculations give the correct sign of the quadrupole deformation for all 4-N nuclei of the S-D shell ; therefore the experimental prolate-oblate transitions are well reproduced. In table II the calculated values of the intrinsic quadrupole moments are compared with those deduced either from measurements of static moments [21-24] or from B(E2) data [35-36] .Since there are occasional discrepancies between the two methods and since the interpretation of the static data (see e.g. Ref.[37]) is somewhat difficult we shall mainly compare our results with those extracted from B(E2) experiments. The absolute values of the charge quadrupole moments calculated with SIII are about 10 to 15 fm^2 lower than experimental ones. As shown in Table II the agreement is systematically better with SIV : with the exception of ^{20}Ne, the calculated moments differ by less than $5fm^2$ from those of the B(E2) data. Such findings could possibly be related to the variation of the effective mass from SIII to SIV. Indeed a decrease of the level density could push to larger deformation the region where the single particle levels cross and thus the appearence of the related shell effect.

There is some experimental evidence that the value of the quadrupole moment of ^{22}Ne is smaller than that of ^{20}Ne. The same holds also for the nuclei ^{26}Mg and ^{24}Mg. Shell model calculations [38] as well as calculations using the Strutinsky prescription [39] fail to reproduce this effect. From table II one sees that our calculations can account for this experimental situation for the Mg isotopes but not for the Ne isotopes. In the case of Mg isotopes our results are a consequence of the following fact : the two additional protons of ^{26}Mg fill mainly the $[202]5/2^+$ oblate state thus reducing the prolate character of ^{24}Mg.

Deformation parameters β_2 and β_4 of a liquid drop having the H.F. quadrupole and hexadecapole moments have been calculated for the charge and the mass densities*. They are reported in Table 12 and in figure 8. The charge and the mass distributions

---

*Such parameters are well known to be dependent on the chosen model for the density, but they are needed for the sake of comparison with optical model analysis data.

have very similar deformation parameters. This could have been expected for such charge-symmetric (or nearly symmetric) nuclei. In fact it was found also to be the case for rare earth and actinide nuclei [14] [16]. In the absence of B(E4) data, the experimental information on hexadecapole moments is only given through mass β_4 values. They have been extracted through optical model analysis of inelastic scattering cross sections of proton [40], ^{3}He [41] and ^{4}He [42] at various energies. Following the conclusion of Ref. [41] some existing data on low energy ^{3}He and ^{4}He scattering have been discarded. We have also eliminated some existing β_4 data concerning the ^{32}S nucleus, since their evaluation was made with a negative sign of the β_2 parameter. The experimental values of β_4 are shown in figure 8. Their trend as a functional of A is fairly well reproduced by our calculations with both interactions. The calculated values of β_4 are negative near the end of the shell. This expected behavior of β_4 [43] has also been obtained in calculations performed with the force SIII in the rare earth and actinide regions [14], [16].

V. Conclusion

In this paper it was shown that simple H.F. calculations using the Skyrme interactions SIII and SIV are able to give correctly some static properties (total binding energies, radii and deformations) of the ground state of S-D shell nuclei. A similar kind of agreement has already been reported for the case of the Na isotopes very far from the bottom of the stability valley [44]. This is all the more significant since effective interactions such as those of the Skyrme type are generally expected to be valid especially for heavy nuclei.

On the average, interactions SIII and SIV reproduce equally well the ground state properties listed above. It is therefore impossible to decide in favor of one of these interactions at this stage. It is possible that this will also be the case for calculation performed in other mass regions (e.g. the rare-earths). Then a direct comparison of the calculated single-particle properties with experiment in spherical and especially in deformed nuclei might still provide a method of determining the non locality of the self-consistent field from an empirical point of view.

Acknowledgments

We would like to express our gratitude to Y. Abgrall, M. Beiner, H. Doubre, S.G. Nilsson, I. Ragnarsson, R. De Swiniarski, J. Vernotte and B.H. Wildenthal for interesting discussions or correspondances and S. Fallieros for a critical reading of the manuscript. The assistance of the Service de calcul de la faculté des sciences d'Orsay is gratefully acknowledged. One of us (P.Q.) would like also to thank the Niels Bohr Institute for the hospitality entended to him and the Statens Naturvidenskabelige Forskningsråd for financial support.

References

1) E.C. Halbert, J.B. Mc Grory, B.H. Wildenthal and S.P. Pandya, in "Adv. in Nucl. Phys." (Plenum, New York, 1971) vol.4
B.H. Wildenthal, J.B. Mc Grory, E.C. Halbert and H.D. Graber, Phys. Rev. C4 (1971) 1708
B.H. Wildenthal, E.C. Halbert, J.B. Mc Grory and T.T.S. Kuo, Phys. Rev. C4 (1971) 1266

2) J. Zofka and G. Ripka, Nucl. Phys. A168 (1971) 65

3) H.C. Lee and R.Y. Cusson, Ann. of Phys. 72 (1972) 353

4) D. Vautherin, Phys. Rev. C7 (1973) 296

5) C. Titin-Schnaider and P. Quentin, Phys. Lett. 49B (1974) 213

6) K. Goeke, J. Garcia and A. Fässler, Nucl. Phys. A208 (1973) 477

7) Y. Abgrall, B. Morand and E. Caurier, Nucl. Phys. A192 (1972) 372

8) H.C. Lee and R.Y. Cusson, Phys. Lett. 39B (1972) 453

9) G. Leander and S.E. Larsson, Nucl. Phys. A239 (1975) 93

10) M. Beiner, H. Flocard, N.V. Giai and P. Quentin, Nucl. Phys. A238 (1975) 29

11) I. Hamamoto, invited talk to the conference on "Hartree-Fock and self-consistent field theories", Trieste (1975)

12) H. Flocard, Phys. Lett. 49B (1974) 129

13) H. Flocard, P. Quentin, A.K. Kerman and D. Vautherin, Nucl. Phys. A203 (1973) 433

14) H. Flocard, P. Quentin and D. Vautherin, Phys. Lett. 46B (1973) 304

15) H. Flocard, P. Quentin, D. Vautherin, M. Veneroni and A.K. Kerman, Nucl. Phys. A231 (1974) 176

16) M. Brack, P. Quentin and H. Flocard, to be published

17) M. Cailliau, J. Letessier, H. Flocard and P. Quentin, Phys. Lett. 46B (1973) 11

18) B. Grammaticos, Thèse 3ème cycle, Université Paris XI (1974), unpublished ; and preprint Saclay DPh.T/74/109

19) D. Vautherin and D.M. Brink, Phys. Rev. C5 (1972) 626

20) C. Titin-Schnaider and P. Quentin, Phys. Lett. 49B (1974) 397

21) D. Schwalm et al., Nucl. Phys. A192 (1972) 479

22) K. Nakai et al., Phys. Rev. Lett. 24 (1970) 903

23) K. Nakai et al., Phys. Lett. 34B (1971) 389

24) A. Olin et al., Nucl. Phys. A221 (1974) 555

25) A.H. Wapstra and N.B. Grove, Nucl. Data A9 (1971) 269

26) W.H. Bassichis, A.K. Kerman and J.P. Svenne, Phys. Rev. 160 (1967) 746

27) M. Sakai, Nucl. Data A10 (1972) 511

28) J.W. Negele, Phys. Rev. C1 (1970) 1260 ;
P. Quentin, Thèse de Doctorat, Université Paris XI (1975), unpublished

29) C.S. Wu and L. Wilets, Ann. Rev. Nucl. Science 19 (1969) 546 ;
Y. Horikawa et al., Phys. Lett. 36B (1971) 9

30) G.C. Li, I. Sick, M.R. Yearien, Phys. Lett. 37B (1971) 282 ;
I. Sick and J.S. Mc Carthy, Nucl. Phys. A150 (1970) 631

31) I. Sick, H. Flocard and M. Veneroni, Phys. Lett. 39B (1972) 443

32) I. Sick, Int. Conf. on Nucl. Structure and spectroscopy (Scholar's press, Amsterdam, 1974) vol.1, page 143

33) M. Arditi, Thèse de doctorat, Université de Paris (1970), unpublished

34) G. Th Kaschl et al., Nucl. Phys. A155 (1970) 417 ;
G. Th Kaschl et al., Nucl. Phys. A136 (1969) 286 ;
P. Doll et al., to be published in Nucl. Phys.

35) D. Schwalm, private communication

36) H. Grawe and P. Lieb, Nucl. Phys. A127 (1969) 13

37) O. Hausser, Journ. Phys. Soc. Japan, Suppl. 34 (1973) 135

38) B.H. Wildenthal, private communication (1973)

39) I. Ragnarsson, private communication (1972)

40) R. De Swiniarski et al., Phys. Rev. Lett. 23 (1969) 317 ;
R. De Swiniarski et al., Phys. Rev. Lett. 28 (1972) 1139 ;
R. De Swiniarski et al., Phys. Lett. 43B (1973) 27 ;
G.M. Crawley et al., Phys. Rev. 160 (1967) 981

41) R. De Swiniarski et al., Journ. de Physique 35 (1974) L25

42) H. Rebel et al., Nucl. Phys. A182 (1972) 145

43) G.F. Bertsch, Phys. Lett. 26B (1968) 130

44) X. Campi, H. Flocard, S. Koonin and A.K. Kerman, to be published ;
H. Flocard, invited talk to the conference on "Hartree-Fock and self-consistent field", Trieste (1975)

45) R. De Swiniarski, private communication (1974)

Table Captions

Table 1 Parameters of the Skyrme interactions SIII and SIV. Notations are those of Ref. [19]

Table 2 Optimal basis parameters

Table 3 Convergence with an increasing size of the basis of H.F. total binding energy for some nuclei of the S-D shell. The number of deformed oscillator shells included in the basis is equal to N+1. The column labelled by ∞ corresponds to spherical H.F. calculation in coordinate space [19]

Table 4 Calculated and experimental (Ref. [29]) total binding energy of some S-D shell nuclei

Table 5 Differences ΔB_S (ΔB) between spherical (deformed) H.F. binding energies and the experimental ones

Table 6 Estimates of the rotational correlation energy $\Delta E = \hbar^2/2\mathcal{J} \langle J^2 \rangle$. The values of moment of inertia extracted from experimental spectra [27] are shown in the first column. The columns $\langle J^2 \rangle$ give the calculated average values of the total angular momentum

Table 7 Experimental (Ref. [29]) and H.F. charge radii

Table 8 Number of nucleons with given L and J a contained in the H.F. intrinsic ground states of the 4-N nuclei of the S-D shell. The results are obtained with the interaction SIII

Table 9 The same as in Table 8 but for the interaction SIV

Table 10 Experimental proton spectroscopic factor. Numbers concerning ^{24}Mg and ^{28}Si are extracted from Ref. [33] and those concerning ^{20}Ne, ^{32}S and ^{36}Ar from Ref. [34]

Table 11 Experimental and calculated proton quadrupole moments Read (1) as : Ref.[35] (2) : Ref.[21] (3) : Ref.[22] (4) : Ref.[24] (5) : Ref.[36] and (6) : Ref.[23]

Table 12 Values of the mass and proton parameters β_2 and β_4 calculated from H.F. quadrupole and hexadecapole moments for the two interactions SIII and SIV.

	t_0 MeV fm^3	t_1 MeV fm^5	t_2 MeV fm^5	t_3 MeV fm^6	x	W MeV fm^5
SIII	-1128.75	395.0	-95.0	14000.0	0.45	120.0
SIV	-1205.6	765.0	35.0	5000.0	0.05	150.0

Table 1

		$b_{(fm^{-1})}$	q			$b_{(fm^{-1})}$	q
^{16}O	spherical	.65	1.0	^{28}Si	prolate	.62	1.07
^{20}Ne	oblate	.64	.85	^{32}S	oblate	.61	.93
	prolate	.64	1.38		prolate	.61	1.24
^{22}Ne	prolate	.64	1.36	^{34}S	oblate	.60	.85
^{24}Mg	oblate	.63	.85		prolate	.60	1.17
	prolate	.63	1.37	^{36}Ar	oblate	.60	0.82
^{26}Mg	prolate	.55	1.39		prolate	.59	1.14
^{28}Si	oblate	.62	.78	^{40}Ca	spherical	.58	1.0

Table 2

Table 3

N	6	8	10	12	∞
^{16}O spherical	126.82	127.40	128.07	128.16	128.17
^{20}Ne prolate	155.31	155.95	156.89	156.99	-
^{36}Ar oblate	300.87	301.15	302.61	302.99	-
^{40}Ca spherical	339.54	339.93	341.49	341.63	341.88

		SIII	SIV	Exp
^{20}Ne	oblate	154.34	151.13	
	prolate	156.89	155.80	160.65
^{22}Ne	prolate	176.99	175.53	177.78
^{24}Mg	oblate	189.60	184.85	
	prolate	195.58	193.56	198.26
^{26}Mg	prolate	214.49	211.17	216.69
^{28}Si	oblate	233.98	231.32	236.54
	prolate	233.27	228.95	
^{32}S	oblate	266.28	260.86	
	prolate	267.30	264.01	271.79
^{34}S	oblate	287.56	283.93	291.85
	prolate	287.24	283.39	
^{36}Ar	oblate	302.607	300.681	306.73
	prolate	300.304	296.532	

Table 4

Table 5

	B exp MeV	ΔB_S SIII MeV	ΔB SIII MeV	ΔB_S SIV MeV	ΔB SIV MeV
^{16}O	127.62	0.59	0.59	0.90	0.90
^{20}Ne	160.65	- 8.61	-3.76	-13.19	-4.85
^{24}Mg	198.26	-10.49	-2.69	-17.14	-4.70
^{28}Si	236.54	- 3.16	-2.56	- 7.69	-5.22
^{32}S	271.79	- 5.45	-4.49	-10.73	-7.78
^{36}Ar	306.79	- 7.26	-4.12	-12.23	-6.059
^{40}Ca	342.06	- 0.18	-0.18	- 0.29	-0.29

		SIII		SIV	
	$\hbar^2/2\mathcal{I}_{(MeV)}$	$\langle J^2 \rangle$	$\Delta E_{(MeV)}$	$\langle J^2 \rangle$	$\Delta E_{(MeV)}$
^{20}Ne prolate	.27	17.82	4.81	19.05	5.14
^{24}Mg prolate	.23	18.22	4.19	18.75	4.31
^{28}Si oblate	.30	11.49	3.45	16.81	5.04
^{32}S prolate	.37	10.64	3.94	13.73	5.08
^{36}Ar oblate	.33	11.14	3.67	13.14	4.34

Table 6

	r^c exp	r^c SIII	r^c SIV
^{20}Ne prolate	2.91	2.967	2.977
^{22}Ne prolate		2.980	2.980
^{24}Mg prolate	3.05 3.01±0.03	3.099	3.097
^{26}Mg prolate		3.070	3.069
^{28}Si oblate	3.14 3.09±0.02	3.168	3.182
^{32}S prolate	3.24±0.02	3.281	3.283
^{34}S oblate		3.302	3.302
^{36}Ar oblate		3.399	3.393

Table 7

Table 8

			neutrons					protons				
	L	J	^{20}Ne P	^{24}Mg P	^{28}Si O	^{32}S P	^{36}Ar O	^{20}Ne P	^{24}Mg P	^{28}Si O	^{32}S P	^{36}Ar O
S	0	1/2	2.3141	2.3586	2.5739	3.0998	3.5336	2.3160	2.3583	2.5739	3.0714	3.5146
P	1	1/2	1.9808	1.9731	1.9841	1.9909	1.9924	1.9804	1.9728	1.9838	1.9908	1.9922
	1	3/2	3.9548	3.9320	3.9631	3.9836	3.9840	3.9540	3.9308	3.9623	3.9830	3.9834
D	2	3/2	0.0956	0.2150	0.2569	0.9826	2.5455	0.0976	0.216	0.2615	1.0142	2.5679
	2	5/2	1.5569	3.3469	5.1165	5.8751	5.8790	1.5524	3.344	5.1108	5.8704	5.8741
F	3	5/2	0.0317	0.0463	0.0264	0.0111	0.0131	0.0321	0.0467	0.0267	0.0145	0.0134
	3	7/2	0.0313	0.0480	0.0259	0.0111	0.0103	0.0321	0.0492	0.0266	0.0115	0.0108
G	4	7/2	0.0046	0.0142	0.0063	0.0111	0.0135	0.0046	0.0142	0.0063	0.0115	0.0139
	4	9/2	0.0282	0.0652	0.0458	0.0311	0.0281	0.0287	0.0662	0.0467	0.0321	0.0290
H	5	9/2	0.0007	0.0002	0.0003	0.0	0.0	0.0008	0.0002	0.0003	0.0	0.0
	5	11/2	0.0005	0.0002	0.0002	0.0	0.0	0.0005	0.0003	0.0002	0.0	0.0

			neutrons					protons				
	L	J	^{20}Ne P	^{24}Mg P	^{28}Si O	^{32}S P	^{36}Ar O	^{20}Ne P	^{24}Mg P	^{28}Si O	^{32}S P	^{36}Ar O
S	0	1/2	2.3338	2.3634	2.7077	2.8512	3.4545	2.3337	2.3642	2.7129	2.8430	3.4482
P	1	1/2	1.9778	1.9672	1.9778	1.9857	1.9889	1.9774	1.9667	1.9774	1.9853	1.9883
		3/2	3.9555	3.9247	3.9522	3.9720	3.9769	3.9546	3.9236	3.9515	3.9711	3.9761
D	2	3/2	0.1694	0.2619	0.4889	1.3364	2.7188	0.1718	0.2629	0.4951	1.3473	2.7286
		5/2	1.4562	3.2975	4.7408	5.7519	5.7788	1.4497	3.2945	4.7278	5.7468	5.7736
F	3	5/2	0.0333	0.0513	0.0347	0.0222	0.0182	0.0337	0.0517	0.0351	0.0227	0.0186
		7/2	0.0313	0.0562	0.0341	0.0200	0.0161	0.0321	0.0574	0.0349	0.0208	0.0168
G	4	7/2	0.0086	0.0150	0.0097	0.0175	0.0149	0.0088	0.0151	0.0098	0.0179	0.0153
		9/2	0.0 310	0.0615	0.0521	0.0426	0.0326	0.0318	0.0628	0.0533	0.0444	0.0339
H	5	9/2	0.0013	0.0003	0.0006	0.0	0.0001	0.0013	0.0003	0.0006	0.0	0.0001
		11/2	0.0007	0.0003	0.0004	0.0	0.0	0.0007	0.0003	0.0004	0.0	0.0

Table 9

	^{20}Ne(1)	^{24}Mg(2)	^{28}Si(2)	^{32}S(1)	^{36}Ar(1)
$2s^{1/2}$	.77	.33	.26	1.62	1.34
$1d^{3/2}$	.49	4.1	5.45	0.68	2.59
$1d^{5/2}$	1.7			2.81	5.59
$1f^{7/2}$	.19				
$1g^{9/2}$					0.22

Table 10

		Q_p SIII	Q_p SIV	$Q_p^{B(E2)}$ exp	$Q_p^{stat.}$ exp
^{20}Ne	oblate	-19.7	-20.25		
	prolate	40.41	43.86	56.4±2.7 (1)	80.5±28 (2)
^{22}Ne	prolate	41.14	43.76	44.7±2.3 (1)	63. ±14 (2)
^{24}Mg	oblate	-24.66	-26.94		
	prolate	55.38	57.20	64.2±1.1 (1)	84. ±21 (2)
^{26}Mg	prolate	40.71	45.32	59.2±8.2 (1)	56. ±14 (2)
^{28}Si	oblate	-42.74	-50.45	57.1±1.1 (1)	-59.5±17.5 (2)
	prolate	10.28	9.46		
^{32}S	oblate	-17.01	-29.42		
	prolate	44.0	50.50	54.3±1.2 (1)	70. ±21 (3) 23. ±6 (4)
^{34}S	oblate	-31.59	-35.36	50.0±4.3 (5)	-9.1±9 (4)
	prolate	34.46	41.22		
^{36}Ar	oblate	-44.04	-47.40	54.0±6.0 (5)	-38.5±21 (6)
	prolate	24.70	25.85		

Table 11

	SIII				SIV			
	β_2^M	β_2^P	β_4^M	β_4^P	β_2^M	β_2^P	β_4^M	β_4^P
^{20}Ne P	.374	.377	.145	.142	.384	.386	.202	.206
^{22}Ne P	.409	.391	.045	.077	.424	.396	.070	.128
^{24}Mg P	.453	.452	-.028	-.025	.467	.472	-.027	-.028
^{26}Mg P	.282	.319	-.009	-.020	.290	.350	-.051	-.025
^{28}Si O	-.303	-.312	.043	.041	-.398	-.403	.097	.100
^{32}S P	.216	.221	-.043	-.048	.273	.277	-.076	-.078
^{34}S O	-.171	-.177	-.021	-.024	-.225	-.217	-.059	-.050
^{36}Ar O	-.222	-.235	-.051	-.056	-.263	-.270	-.088	-.092

Table 12

Figure Captions

Figure 1 — Differential cross section of elastic electron scattering ^{28}Si. The solid and dashed line are obtained by a phase shift analysis using the monopole part of the calculated charge densities. Experimental points are taken from Ref. [30].

Figure 2 — The same as in Fig.1 but for the ^{32}S nucleus.

Figure 3 — Mean percentage deviation (see text) from experimental data on ^{28}Si. The deviation is plotted as a function of the effective momentum transfer as it is defined in Ref. [30].

Figure 4 — The same as in Fig.3 but for the nucleus ^{32}S

Figure 5 — Differences between charge densities of ^{32}S and ^{28}Si. The dashed curve corresponds to spherical H.F. densities calculated with SIII. The solid (dotted) line is obtained from deformed H.F. calculations with SIII (SIV).

Figure 6 — Single neutron spectra of 4-N nuclei

Figure 7 — Single proton spectra of 4-N nuclei

Figure 8 — Comparison of values of B_4 deduced from H.F. multipole moments with those extracted from optical model analysis. Black, black and white and white squares correspond to (p-p') experiments (Refs.[40]). The data stemming from (^{3}He-$^{3}He'$) experiments are indicated by black points (Ref.[41]) and (^{4}He-$^{4}He'$) Ref.[42] values are shown by triangles. The main part of the dispersion of experimental results can probably be corrected by taking into account the different sizes of the used projectiles [45].

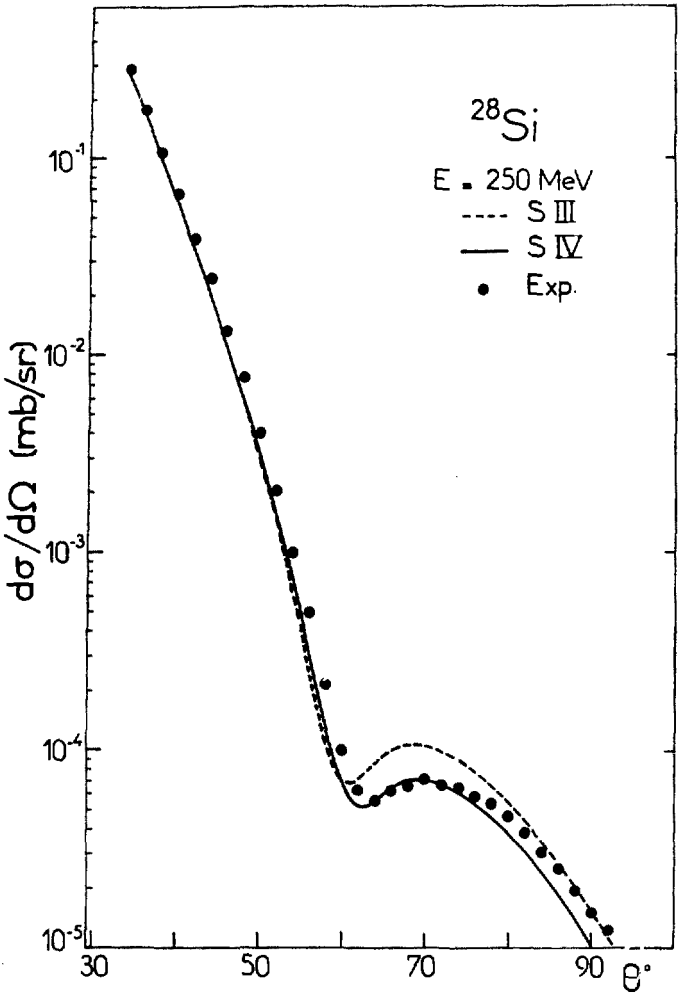
^{28}Si
E = 250 MeV
---- S III
—— S IV
• Exp.
$d\sigma/d\Omega$ (mb/sr)
10^{-1}
10^{-2}
10^{-3}
10^{-4}
10^{-5}
30
50
70
90
θ°

Fig.1

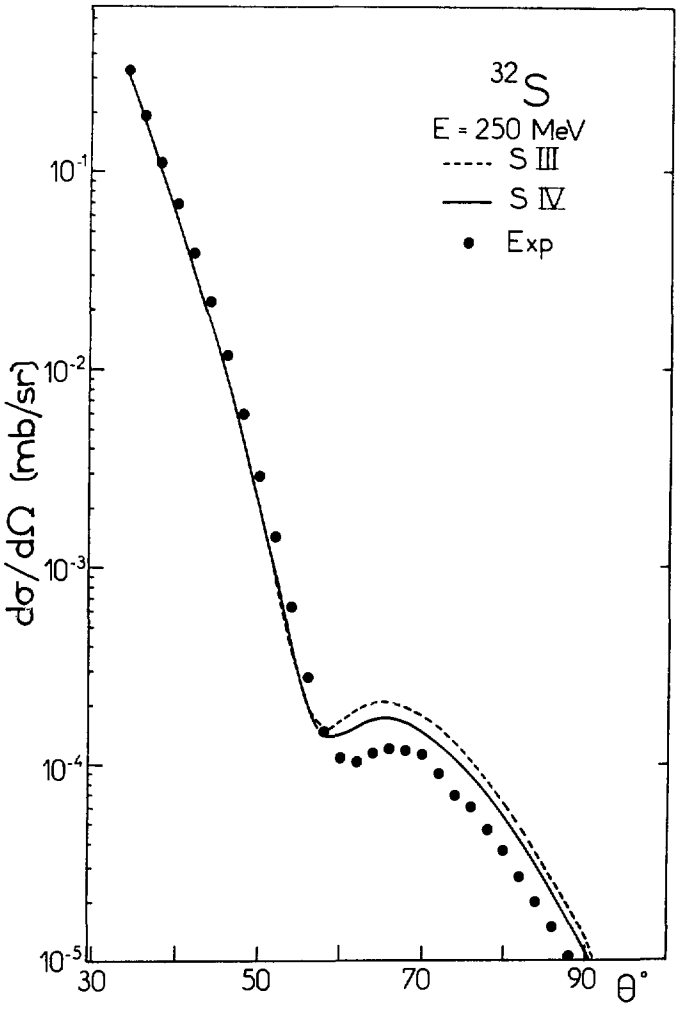
^{32}S
E = 250 MeV
S III
S IV
Exp
$d\sigma/d\Omega$ (mb/sr)
10^{-1}
10^{-2}
10^{-3}
10^{-4}
10^{-5}
30
50
70
90
θ°

Fig.2

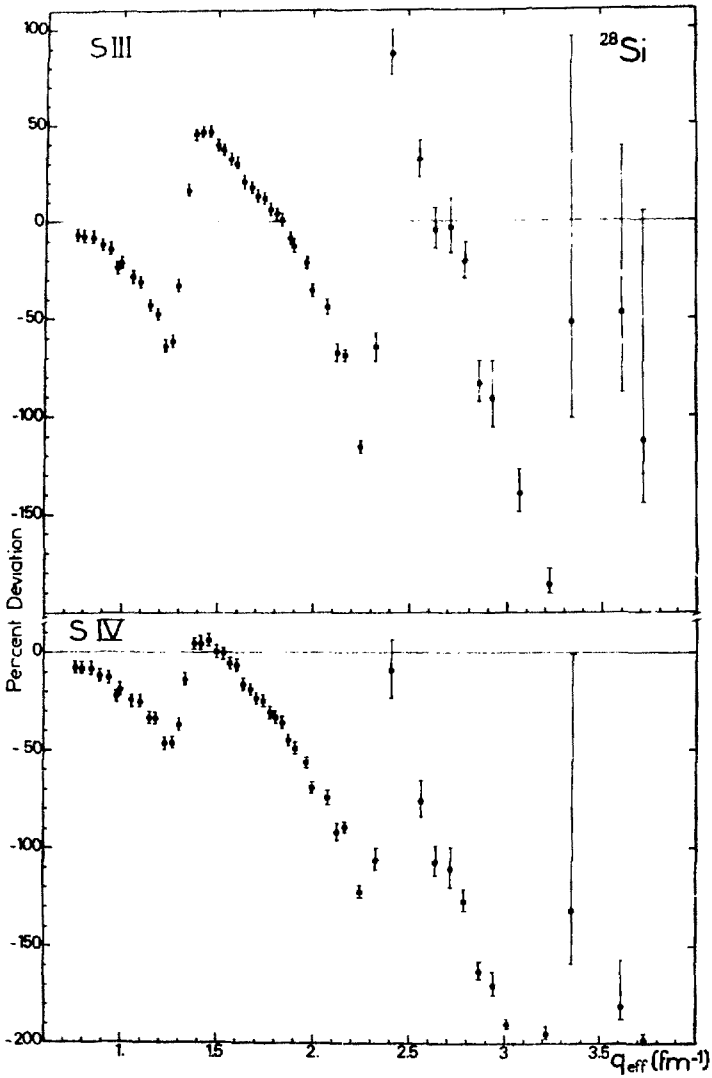
S III
^{28}Si
S IV
Percent Deviation
100
50
0
-50
-100
-150
-200
1.
1.5
2.
2.5
3
3.5
q_{eff} (fm^{-1})

Fig.3

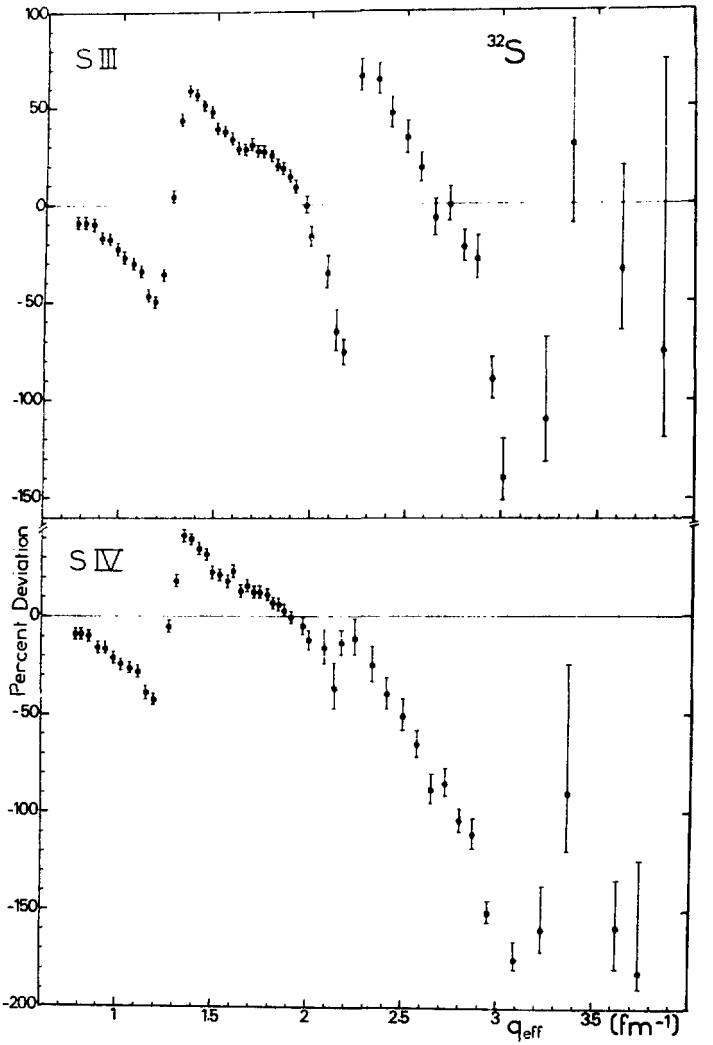
S III
^{32}S
S IV
Percent Deviation
100
50
0
-50
-100
-150
-200
1
1.5
2
2.5
3
3.5
q_{eff} (fm^{-1})

Fig.4

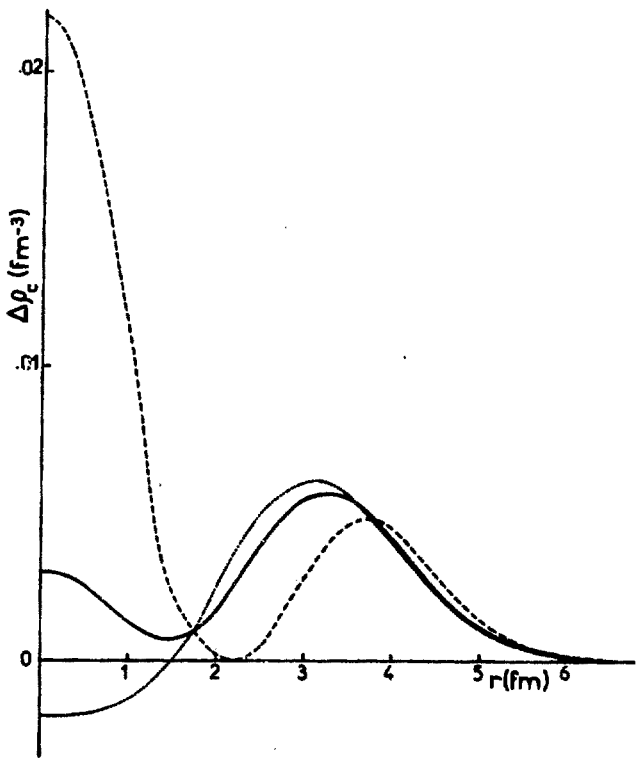

Fig.5

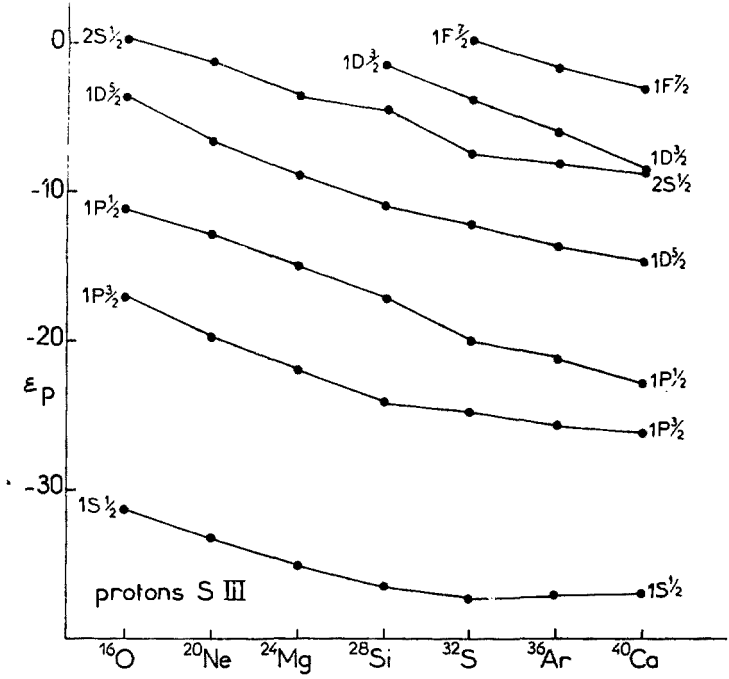
0
-10
-20
-30
ε_p
$2S_{1/2}$
$1D_{5/2}$
$1P_{1/2}$
$1P_{3/2}$
$1S_{1/2}$
$1F_{7/2}$
$1D_{3/2}$
protons S III
^{16}O
^{20}Ne
^{24}Mg
^{28}Si
^{32}S
^{36}Ar
^{40}Ca

Fig.6

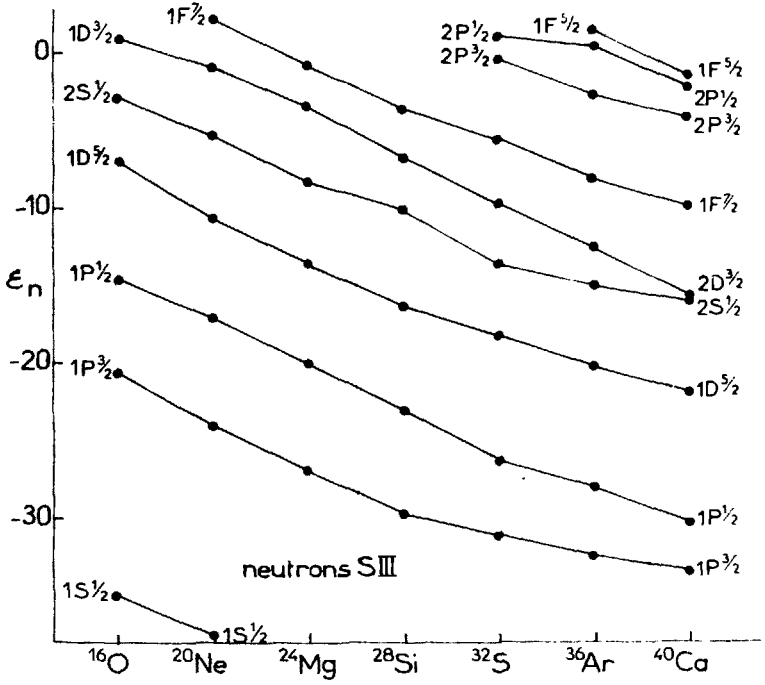
0
-10
-20
-30
ε_n
1D3/2
2S1/2
1D5/2
1P1/2
1P3/2
1S1/2
1F7/2
2P1/2
2P3/2
1F5/2
neutrons SIII
16O
20Ne
24Mg
28Si
32S
36Ar
40Ca

Fig.7

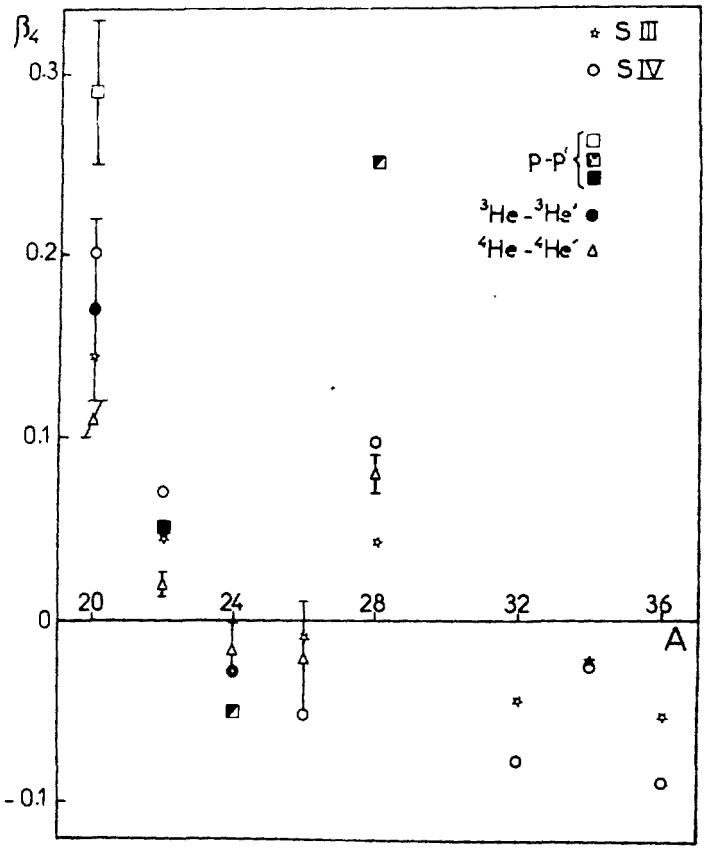

Fig.8